Food and Bioprocess Technology (2026) 19:319
https://doi.org/10.1007/s11947-026-04394-y

RESEARCH

Electrospun Wheat Starch Nanofibers for Encapsulation of Chlorogenic Acids from the By-product of Yerba Mate (*Ilex paraguariensis*)

Felipe Nardo dos Santos[1] · Yasmin Völz Bezerra Massaut[2] · Alexandra Gomes Lizandra Rosas[2] · Laura de Vasconcelos Costa[2] · Thaís Regina Rodrigues Vieira[2] · Thamyres Cesar de Albuquerque Sousa[2] · Igor Henrique de Lima Costa[1] · Helen Cristina dos Santos Hackbart[2] · Elessandra da Rosa Zavareze[1] · Adriana Dillenburg Meinhart[2]

Received: 14 January 2026 / Accepted: 5 May 2026 / Published online: 16 May 2026
© The Author(s) 2026

Abstract

The agricultural co-product generated from the pruning and harvesting of yerba mate (*Ilex paraguariensis*) is a rich source of chlorogenic acids, bioactive compounds sensitive to light and temperature that require protection to preserve their antioxidant activity. In this study, electrospinning was used to encapsulate chlorogenic acids from an optimized *I. paraguariensis* co-product extract into wheat starch nanofibers. The extract was incorporated at concentrations of 0%, 5%, 10%, and 15% (w/w), resulting in continuous, homogeneous nanofibers with smooth surfaces and average diameters ranging from 195 to 218 nm. Increasing extract concentration led to higher viscosity and electrical conductivity, contributing to the formation of thicker nanofibers. Encapsulation efficiency ranged from 90.8 to 63.7%, with the highest value observed for nanofibers whit 5% of extract. The nanofibers exhibited antioxidant activity against $ABTS^{\bullet+}$ and DPPH radicals, indicating partial preservation of bioactivity after encapsulation. Thermogravimetric analysis demonstrated increased thermal resistance of the encapsulated compounds compared to the free extract, confirming the protective effect of the starch matrix. The nanofibers showed a controlled release profile of chlorogenic acids, with slower release in hydrophilic media (10% ethanol) and faster release under lipophilic conditions (50% ethanol), highlighting their potential for different food applications. FTIR analysis confirmed interactions between extract compounds and starch, while contact angle measurements suggested increased hydrophilicity. Overall, wheat starch nanofibers proved to be an efficient and sustainable matrix for encapsulation and controlled delivery of bioactive compounds, contributing to the valorization of yerba mate co-products within a circular economy approach.

Keywords Agricultural co-product · Bioactive compounds · Antioxidants · Sustainable materials

✉ Felipe Nardo dos Santos
felipe22.s@hotmail.com

Yasmin Völz Bezerra Massaut
yasmin_vbm@hotmail.com

Alexandra Gomes Lizandra Rosas
lizandra.rosas2015@gmail.com

Laura de Vasconcelos Costa
lauravcosta98@hotmail.com

Thaís Regina Rodrigues Vieira
thattyvieira04@gmail.com

Thamyres Cesar de Albuquerque Sousa
thatahcesar@gmail.com

Igor Henrique de Lima Costa
igorhenr.98@gmail.com

Helen Cristina dos Santos Hackbart
helenhackbart@gmail.com

Elessandra da Rosa Zavareze
elessandrad@yahoo.com.br

Adriana Dillenburg Meinhart
adrianadille@gmail.com

[1] Department of Agroindustrial Science and Technology, Laboratory of Biopolymers and Nanotechnology in Food (BioNano), Graduate Program in Food Science and Technology, Federal University of Pelotas, Pelotas 96010-900, Brazil

[2] Department of Food Science and Agrotechnology, Federal University of Pelotas, Pelotas 96010-900, Brazil

Introduction

With the high demand from consumers for healthier products, the food industry is increasingly focused on developing innovative technologies to meet this demand and ensure more nutritious and safer foods for human consumption (Oliveira et al., 2020). Polymeric nanofibers are used to produce nano- or microscale materials and, in the food sector, they enhance desirable properties, preserve the physicochemical stability of molecules, and enable the controlled release of bioactive compounds (Kim et al., 2016; Pires et al., 2023, 2024a).

Electrospinning is a simple, cost-effective, and efficient technique for producing polymeric nanofibers, widely applied to encapsulate bioactive compounds, protecting them from environmental factors and masking undesirable sensory attributes (Lim, 2020; Lim et al., 2019). The parameters used in the technique can be controlled, forming nanofibers with different morphologies as desired (Ashraf et al., 2019).

Different materials can be used, and among the natural polymers employed are zein (Santos et al., 2023), gelatin (Etxabide et al., 2022), cyclodextrin (Topuz & Uyar, 2020), and starches (Fonseca et al., 2025). Starch is abundant in nature, low-cost, easy to obtain, edible, and biodegradable. It is currently being studied as a wall material in the electrospinning technique for the encapsulation of bioactive compounds such as orange essential oil (Santos et al., 2025), curcumin (Pires et al., 2022), red onion extract (Cruz et al., 2023), and carvacrol (Fonseca et al., 2019). However, it has limitations due to its hydrophilic nature and inferior mechanical properties compared to other materials.

Starches with higher amylose content exhibit improved electrospinning performance, as the random coil conformation of amylose chains provides better entanglement, which is crucial for fiber formation (Fonseca et al., 2019; Mendes et al., 2017). High-amylose corn starch nanofibers were produced and showed regularity, with a smooth and continuous structure (Kong & Ziegler, 2012); similarly, potato soluble starch nanofibers for thyme essential oil encapsulation exhibited homogeneous morphology, high encapsulation efficiency (99.1%–99.8%), and strong protection of the compounds (Fonseca et al., 2020a). Among the different types of starch, wheat starch stands out for its high amylose content, which gives it great potential for fiber production; however, it has not yet been explored for the encapsulation of bioactive compounds by electrospinning.

Ilex paraguariensis is a plant native to South America popularly known as yerba mate, mainly used in beverages produced from its leaves and small branches (Godoy et al., 2013; Mesquita et al., 2021; Vieira et al., 2023). The plant contains high concentrations of bioactive compounds, mainly phenolic acids, and its beneficial effects have been reported in relation to antioxidant, anti-inflammatory, hypolipidemic, hypocholesterolemic, antimicrobial, hypoglycemic, anticancer, and anti-obesogenic activities (Ali et al., 2017; Garcia-Lazaro et al., 2020; Kungel et al., 2018; Mesquita et al., 2021; Santiano et al., 2023; Uecker et al., 2019).

During the harvest of *I. paraguariensis*, the plant is pruned in order to reduce its height and enable the next harvest (Lorini et al., 2021). This pruning generates co-product consisting of stems larger than 10 mm in diameter, which are not yet used in commercial products. Studies on the bark of this plant have demonstrated great potential due to the presence of secondary metabolites (chlorogenic acids) in amounts similar to those found in the leaves and thin stems (Pagliosa et al., 2010). Chlorogenic acids are sensitive to light, oxygen, and high temperatures, requiring alternatives that enhance their stability and preserve their biological function throughout processing (Tarahi et al., 2024).

The literature reports encapsulation techniques for *I. paraguariensis* extract through the development of biodegradable and edible films using cassava starch (Jaramillo et al., 2016), and electrospinning using zein as the polymeric material (Bruni et al., 2020). However, there are still no reports on the production of polymeric nanofibers from wheat starch for the encapsulation of bioactive compounds derived from *I. paraguariensis* bark. For this reason, the aim of this study was to produce and characterize wheat starch nanofibers by the electrospinning technique as an alternative for the protection and preservation of chlorogenic acids present in the optimized aqueous extract of the *I. paraguariensis* co-product.

Materials and Methods

Materials

The bark, the outer part of the co-product generated during the pruning of *I. paraguariensis* from thick stems for obtaining *I. paraguariensis* co-product (cultivate Cambona 4), was obtained from the Association of Yerba Mate Producers of Machadinho/RS/Brazil (27°32′35.5″S; 51°39′46.9″W), from a sun-grown plantation. Commercial wheat flour (Tordilho, Pelotas, Brazil) was purchased from the local market in Pelotas/RS/Brazil. Methanol of chromatographic grade was acquired from Honeywell (Wabash, USA). The standards of chlorogenic acids 3-caffeoylquinic acid (3-CQA), 4-caffeoylquinic acid (4-CQA),

5-caffeoylquinic acid (5-CQA), 3,4-dicaffeoylquinic acid (3,4-DQA), 3,5-dicaffeoylquinic acid (3,5-DQA), and 4,5-dicaffeoylquinic acid (4,5-CQA) were obtained from Biopurify (Chengu, China). The standards were diluted in methanol (1 mg/mL) and stored in an ultrafreezer at − 70 °C for a maximum of two days. All solutions and mobile phases were filtered using nylon membranes with a porosity of 0.22 µm (Analítica, São Paulo, Brazil). Formic acid (methanoic acid) was used as the solvent (purity: 85%, Synth, CAS 01A1034.01) for fiber formation. Ultrapure water was obtained using MecLab's MegaPurity® system. All other reagents used were of analytical grade.

Preparation of the Co-product and Aqueous Extract

After obtaining the co-product, the bark was dried in a forced-air oven at 135 °C for 24 h (Schifel, Erechim, Brazil). Following drying, the material was ground for 5 min (1200 W) using a domestic blender (ProBlend 6, Philips Walita, Brazil), sieved through a 50-mesh screen, and stored in sealed plastic packages at room temperature in a dry place until analysis. The preparation of the aqueous extract of the *I. paraguariensis* co-product was carried out according to the method described by Paim et al. (2024), an amount of 0.25 g of co-product was dissolved in 30 mL of mineral water and placed in amber vials hermetically sealed. The vials were heated in a water bath (Velp Scientifica, Enzymatic Digester-GDE, Italy) at 30 °C under magnetic stirring for 5 min. The extracts were filtered through quantitative filter paper (180 µm), frozen in an ultra-freezer (−70 °C) for 24 h, and lyophilized (Liotop K108, Brazil) under the following conditions: 105 µHg, − 62 °C, 203 Vca, for 72 h. Afterwards, they were stored in hermetically sealed plastic packages at room temperature (25 °C) until analysis, the extract was coded as IPE (*Ilex paraguariensis* extract).

Characterization of the Phenolic Compounds

The analysis of chlorogenic acids, including 5-caffeoylquinic acid (5-CQA), 3-caffeoylquinic acid (3-CQA), 4-caffeoylquinic acid (4-CQA), 3,4-dicaffeoylquinic acid (3,4-DQA), 3,5-dicaffeoylquinic acid (3,5-DQA), and 4,5-dicaffeoylquinic acid (4,5-DQA) was performed using high-performance liquid chromatography with a diode array detector (UFLC, Shimadzu, Japan) operating at 325 nm. The system was equipped with an automatic injector, a quaternary pump, and a Cogent 2.0 Bidentate C18 column (MicroSolv Technology Corp., Leland, NC, USA) with dimensions of 2.1 mm i.d., 100 mm length, and 2.2 µm particle size. The column was maintained at a temperature of 40 °C. The analysis method was based on the one described by Lorini et al. (2021). The elution was performed using a gradient system starting with 99% of solvent A (water acidified with 0.1% formic acid) and 1% of solvent B (methanol). The gradient increased linearly until reaching 36% of solvent B at 35 min and was maintained for 2.5 min. From 37.5 to 40 min, the gradient reached 100% of solvent B and was maintained for 1 min for column cleaning purposes. Next, the column was reconditioned with the initial mobile phase composition for 5 min. The flow rate of the mobile phase was set at 0.2 mL/min, and the injection volume was 10 µL. The identification of chlorogenic acids was performed by comparing the retention time, diode array detector (DAD) absorption spectrum, and co-chromatography with an analytical standard.

The method validation included parameters such as the limit of detection, limit of quantification, linearity, intraday precision, and interday precision, following the guidelines of the International Union of Pure and Applied Chemistry (Thompson, Ellison, & Wood, 2002). The validation results were found to be suitable for the analysis. The results were expressed as chlorogenic acids concentration (g/100 g in the co-product).

Extraction of Wheat Starch, Yield, Moisture, and Amylose

Wheat starch was extracted according to the method described by Baranzelli et al. (2019), with adaptations. For this, wheat flour was added to a saline solution at a 2:1 ratio (w/v; 1000 g of flour and 500 mL of 2% sodium chloride solution) and left to rest in a container covered with distilled water for approximately 30 min. After this period, the dough was washed with distilled water until complete removal of the starch. The starch suspension was sieved (200 mesh sieve), centrifuged (Eppendorf Centrifuge 5430 R, Germany) at 6500 × g for 10 min, and the supernatant was discarded. The decanted material was resuspended in distilled water (this procedure was performed three times). The resulting starch was dried in an air-circulating oven at 40 °C for 24 h and, subsequently, the starch was ground in a knife mill (Oster, OMDR100/Brazil), sieved (50 mesh sieve), and stored in a sealed plastic container until analysis. The yield was calculated as the percentage of starch mass obtained in relation to the raw mass of the flour used, and the moisture content according to Association of Official Analytical Chemists (AOAC, 2005); the samples were dried in an oven at 105 °C until constant weight was obtained, and the analysis was performed in triplicate. The amylose content was determined following the method of Chen et al., (2021) with adaptations. Initially, 30 mg of wheat starch was weighed and completely dispersed in a test tube with 400 µL of 95% ethanol solution and 3.6 mL of 1 M sodium hydroxide solution. The mixture was vortexed for 10 s and then heated in a boiling water bath (Velp Scientifica, Enzymatic Digester-GDE, Italy) at ≈ 85 °C for 10 min

to achieve complete starch gelatinization. Afterward, the mixture was cooled to room temperature (25 °C), 25 mL of deionized water and 3.8 mL of Lugol's solution (2.00 g of potassium iodide and 0.200 g of iodine per 100 mL of solution) were added to 200 µL of the test solution, stirred, and left to stand for 10 min. The absorbance of the solution was measured at 620 nm, adjusting the spectrophotometer (Molecular Devices, SpectraMax 190, USA) to zero with 0.09 M sodium hydroxide. The standard curve was prepared using potato starch with a known amylose content. The amylose content in the sample was calculated according to the absorbance value and the standard curve.

Production of Wheat Starch Nanofibers by the Electrospinning Technique

Preparation of Polymer Solutions and Electrospinning Process

Initially, the study was divided into two stages. In the first stage, the parameters were evaluated to define the starch concentration capable of producing nanofibers. Polymer solutions were prepared with different starch concentrations (15%, 20%, and 30%; w/v) diluted in formic acid at 75% and 85% (w/v). The process parameters were also adjusted by varying the pumping flow rate (0.8 and 1.0 mL/h), while the distance and applied voltage were fixed at 20.5 cm and 23 kV, respectively, based on preliminary tests (Pires et al., 2024a). From this stage, the condition selected for nanofibers production was the solution containing 15% wheat starch and 75% formic acid (w/v). In the second stage, different concentrations of lyophilized IPE co-product (5%, 10%, 15%, 20%, and 30%; w/w) were incorporated into the previously established starch solution in order to determine the maximum concentration that could be added without compromising nanofibers formation. Additionally, different solution flow rates during the electrospinning process (0.6, 0.8, and 1.0 mL/h) were evaluated. Based on the obtained results, the concentrations of 5%, 10%, and 15% (w/w), at a flow rate of 0.8 mL/h, were selected for the subsequent study.

Thus, the final conditions used for nanofibers production consisted of a polymer solution containing 15% starch (w/v). After 24 h of agitation, the IPE was added at concentrations of 5%, 10%, or 15% (w/w), and the solution was further stirred for 30 min prior to the electrospinning process. The polymer solutions were individually placed in 3 mL plastic syringes coupled to a stainless-steel needle with a diameter of 0.8 mm. The production of the nanofibers was carried out in an electrospinning station composed of a high-voltage power supply (INSTOR, INSES-HV30, Brazil), an infusion pump (KD Scientific, Model 100, Holliston, UK), and a stainless-steel collector covered with aluminum foil for material deposition (Santos et al., 2025). The parameters defined and used for the electrospinning process were a pumping flow rate of 0.80 mL/h, an applied voltage of 23 kV, and a distance of 20.5 cm. The relative humidity was maintained at 45 ± 5%, and the temperature at 23 ± 2 °C.

Characterization of Polymer Solutions—Electrical Conductivity and Rheological Properties

The polymer solutions, with and without IPE, were characterized in terms of electrical conductivity and rheological properties only under the selected optimal conditions, namely 15% starch (w/v) and IPE concentrations of 5%, 10%, and 15% (w/w). For the determination of electrical conductivity, 5 mL aliquots of each solution were analyzed in triplicate at room temperature (20 ± 1 °C) using a benchtop conductivity meter (Tecnopon, mCA 150P, Brazil). The results were expressed in mS/cm (Santos et al., 2024a). Rheology was used to determine the viscosity of the polymer solutions. For this purpose, a rheometer (Rheostress RS 150, Germany) coupled to a temperature controller (Haake DC 50, Germany) was employed. A rotational shear deformation was applied with a shear rate of 0.1–100 s^{-1} for 300 s at 25 °C. The Herschel–Bulkley model was chosen to obtain the rheological parameters using Eq. (1), where τ is the shear stress (Pa), τ_0 is the yield stress (Pa), κ is the consistency index (Pa·s), $\dot{\gamma}$ is the shear rate (s^{-1}), and n is the flow behavior index, according to the methodology proposed by Santos et al. (2024a).

$$\tau = \tau^0 + k(\dot{\gamma})^n \quad (1)$$

Oscillatory shear analysis was performed through frequency sweep tests, in which changes in the viscoelastic modulus were evaluated as a function of frequency (0.1–10 Hz). Preliminary amplitude sweep tests confirmed the use of 1% strain within the linear viscoelastic region. A cone-plate geometry was employed, with a rotating cone of 60 mm diameter, 2° angle, and 0.105 mm gap.

Morphology and Size Distribution of Nanofibers

The initial tests were optically characterized to determine the best conditions for producing uniform nanofibers, with or without the addition of IPE extract. The optical characterization of the electrospinning nanofibers was performed using an optical microscope (BIOPTIKA B10, Italy) equipped with a digital camera coupled to the eyepiece. The analyses were conducted without polarization, and the samples were observed at appropriate magnifications to evaluate the general morphology of the nanofibers. The images obtained were used to qualitatively

assess the uniformity, continuity, and distribution of the nanofibers, as well as the presence or absence of defects such as beads or aggregates. The recorded micrographs allowed for the comparison between different formulations, providing a visual evaluation of the effect of IPE incorporation on the nanofibers structure.

Based on these preliminary analyses, the morphology of the nanofibers was further evaluated by scanning electron microscopy (SEM) (Jeol, JSM-6610LV, USA) only for the selected optimal conditions (15% starch (w/v) with IPE concentrations of 5%, 10%, and 15% (w/w), as well as the control sample without extract). For SEM analysis, a portion of the material deposited on aluminum foil was fixed on sample holders using double-sided carbon tape and coated with gold using a sputter coater (Denton Vacuum Desk V, USA). The samples were analyzed at an accelerating voltage of 10 kV, and micrographs were obtained at magnifications of × 1000 and × 5000. The average fiber diameter and size distribution were determined from the images by measuring seventy randomly selected fiber segments using ImageJ© software (version 2015) (Santos et al., 2024b).

Encapsulation Efficiency

The encapsulation efficiency (EE) of wheat starch nanofibers encapsulated with IPE was evaluated according to the method described by Cruz et al. (2023), with adaptations. Nanofibers samples (10 mg) were weighed, and 800 µL of formic acid solution (75%, in ultrapure water, v/v) was added. The mixture was vortexed for 2 min and subsequently 2.2 mL of acetonitrile:ultrapure water solution (1:1 v/v) was added, vortexed for 30 s, and centrifuged (Eppendorf Centrifuge 5430 R, Germany) for 10 min at 4 °C and 6000 rpm. The samples were analyzed using a spectrophotometer (Jenway Model 6705 Scanning UV/Visible Spectrophotometers) at 325 nm. The identification of the compounds present in the nanofibers was confirmed by comparison with the non-encapsulated compound. The EE was expressed as a percentage (%) and calculated according to Eq. 2:

$$EE\ \% = \frac{Amount\ of\ compound\ present\ in\ the\ nanofibers}{Amount\ of\ compound\ added\ in\ the\ nanofibers} \times 100 \quad (2)$$

Functional Groups

The functional groups were identified by Fourier-transform infrared spectroscopy (FTIR). The analyses were performed on both the nanofibers and the pure extract (IPE), using an FTIR IRAffinity^{-1} spectrometer (ATR, Shimadzu) within the resolution range of 400–4000 cm^{-1} (Torres et al., 2025). A sufficient amount of sample was applied to cover the crystal of the equipment, and 60 scans were performed with Happ-Genzel apodization. Data acquisition, expressed in wavenumbers, was carried out using the IRsolution software, version 1.60 (Shimadzu Corporation).

Thermal Properties

The thermal properties of the nanofibers and the pure extract (IPE) were measured using a thermogravimetric analyzer (TA-60WS, Shimadzu, Kyoto, Japan). Approximately 5 mg of nanofibers and pure compounds were heated in platinum pans from 30 to 600 °C under a nitrogen atmosphere with a flow rate of 50 mL/min, starting at 30 °C and using a heating rate of 10 °C/min until reaching the final temperature of 600 °C (Souza et al., 2024).

Contact Angle

Wheat starch nanofibers containing different concentrations of IPE were evaluated for wettability using the sessile drop technique by measuring the static contact angle (θ) with an optical tensiometer (Theta Lite, Biolin Scientific, model TL100, SE). To determine θ between the nanofibers membrane and ultrapure water, seven µL droplets ($n = 3$) were deposited onto glass slides containing the fiber samples. Water absorption by the nanofibers was recorded using the equipment's digital camera at 20 FPS (frames per second), from time zero up to 20 s (Santos et al., 2023).

Antioxidant Activity

The antioxidant activity of the nanofibers with and without the extract was evaluated against the 2,2-diphenyl-1-picrylhydrazyl radical (DPPH), and against the 2,2′-azino-bis-(3-ethylbenzothiazoline-6-sulfonic acid) radical ($ABTS^{\bullet+}$) (Santos et al., 2023). For the DPPH method, one mg of samples was weighed into falcon tubes and 3.9 mL of DPPH solution (prepared with methanol and adjusted to an absorbance of 1.10 ± 0.02) was added, followed by vortex mixing for 30 s. The samples were then kept in the dark at room temperature (22 ± 2 °C) for 2 h and 30 min. The absorbance of the samples was measured at 515 nm using a spectrophotometer (Jenway Model 6705 Scanning UV/Visible Spectrophotometers). The antioxidant activity against the DPPH radical was calculated and expressed as % inhibition using Eq. 3:

$$Inhibition\ (\%) = \frac{Abs_{blank} - Abs_{sample}}{Abs_{blank}} \times 100 \quad (3)$$

For the antioxidant activity against the $ABTS^{\bullet+}$ radical, 5 mL of $ABTS^{\bullet+}$ stock solution (7.4 mM) was mixed with 88 µL of sodium persulfate (140 mM) and kept in the dark for 16 h at room temperature (22 ± 2 °C). The solution was then diluted with ethanol to adjust the absorbance to 0.70 ± 0.05 at 734 nm. Subsequently, 1 mg of sample was weighed into Falcon tubes and 3 mL of the $ABTS^{\bullet+}$ solution was added. The mixtures were vortexed for 30 s and then kept in the dark for 30 min at room temperature (22 ± 2 °C). The absorbance of the samples was measured at 734 nm (Jenway Model 6705 Scanning UV/Visible Spectrophotometers), and the results were expressed as percentage inhibition according to Eq. 3.

Simulation of the In Vitro Release of Chlorogenic Acids Present in Nanofibers

The release of phenolic compounds was evaluated using food simulants corresponding to categories A (10% ethanol) and D1 (50% ethanol), as established by Commission Regulation (EU) (2011), which addresses plastic materials and articles intended to come into contact with food, following the methodology proposed by Cruz et al. (2023). The analysis was carried out to assess the release of chlorogenic acids from wheat starch nanofibers. For this purpose, ten mg of each sample of nanofibers, at concentrations of 5, 10, and 15% (w/w) of IPE were used. The samples were individually immersed in 3 mL of each food simulant and kept for 24 h at room temperature (± 23 °C). After this period, the released chlorogenic acids were quantified by HPLC, as described in Sect. "Characterization of the Phenolic Compounds", and the results were expressed as a percentage according to Eq. 4.

$$Release\ (\%) = \frac{Amount\ of\ compounds\ in\ the\ simulant\ medium}{Amount\ of\ compounds\ in\ the\ nanofibers} \times 100 \quad (4)$$

Thermal Resistance of Chlorogenic Acids Encapsulated in Nanofibers

The thermal resistance of wheat starch nanofibers containing different concentrations of IPE (5, 10, and 15%, w/w) was evaluated according to the methodology proposed by Cruz et al. (2023), with minor modifications. Briefly, fiber samples (10 mg) were weighed into glass vials and subjected to thermal treatment in a forced-air circulation oven set at 120 °C for 1 h. Subsequently, the nanofibers were disrupted using 75% formic acid (1 mL) and vortexed for 1 min. Then, 2 mL of water was added for the extraction of chlorogenic acids, and the solution was vortexed again for 1 min. Finally, the samples were centrifuged at 3000 rpm for 5 min at 4 °C. After this period, the released chlorogenic acids were quantified by HPLC, as described in Sect. "Characterization of the Phenolic Compounds", and the results were expressed as a percentage according to Eq. 5.

$$Thermal\ resistance\ (\%) = \frac{Stable\ compound\ amount}{Amount\ of\ compounds\ in\ the\ nanofibers} \times 100 \quad (5)$$

Principal Component Analysis

Principal component analysis (PCA) was carried out on the dataset related to the nanofibers (regarding average diameter, encapsulation efficiency, water contact angle, and antioxidant activity against DPPH and $ABTS^{\bullet+}$ radicals) based on the correlation matrix using Statistica software (version 7.0). Principal components (PC) 1 and 2 were selected for plotting the loadings and scores, as they accounted for a cumulative total variance of 94.29%, according to factor analysis.

Statistical Analysis

The results were evaluated by analysis of variance (ANOVA) using Statistica software (version 7.0), with Tukey's test as a post oc procedure, at a 95% significance level.

Results and Discussion

Characterization of the Phenolic Compounds

Chlorogenic acids identified in the extract obtained from the bark (outer fraction) of the co-product generated during the pruning of thick stems of *Ilex paraguariensis* (Cambona 4 cultivar) included mono- and dicaffeoylquinic acid isomers. Among the caffeoylquinic acids (CQA), 3-CQA (1.27 ± 0.01 g/100 g), 5-CQA (1.41 ± 0.01 g/100 g), and 4-CQA (1.27 ± 0.01 g/100 g) were quantified. Among the dicaffeoylquinic acids (DQA), 3,4-DQA (0.24 ± 0.01 g/100 g), 3,5-DQA (1.55 ± 0.01 g/100 g), and 4,5-DQA (1.62 ± 0.02 g/100 g) were identified. The total content of these compounds was 7.36 ± 0.07 g/100 g, indicating a high concentration of chlorogenic acids in the liquid extract. After the freeze-drying process, the chlorogenic acid content was 27.98 g of freeze-dried extract per 100 g of co-product. In a study conducted by Lorini et al. (2021), evaluating different parts of *Ilex paraguariensis* (leaves, thin stems, and thick stems), the chlorogenic acid content in thick stems was reported to be approximately 3.4 g/100 g using an exhaustive extraction process with methanol/water, which is about two times lower than the

value observed in the present study, using only water as the extraction solvent. This difference may be associated with the evaluated fraction (bark), which can concentrate higher levels of secondary metabolites, as well as differences in extraction methods and raw material conditions. Furthermore, the high phenolic content found in this residue is greater than that reported for several plant-based matrices, including 64 fruits, 53 vegetables, and 99 teas, as described by Meinhart et al., (2017, 2019) highlighting the strong potential of this material as a source of bioactive compounds. In this context, the total content of 7.36 g/100 g obtained in this study further reinforces the potential of yerba mate pruning co-product bark as a highly concentrated source of chlorogenic acids, with possible applications in food matrices as well as in the pharmaceutical and cosmetic industries.

Yield, Moisture, and Amylose Content of Wheat Starch

The extraction of starch from wheat flour resulted in a yield of 41.68%. Starch is the major component of the wheat endosperm, typically accounting for 70–75% of the grain, while the remaining fraction consists mainly of proteins and minor constituents (Filip et al., 2023). Variations in extraction yield are commonly associated with differences in processing conditions, flour composition, and the efficiency of starch separation techniques (Wang et al., 2020).

The wheat starch presented a moisture content of 7.49% ± 0.06, which is well below the maximum limit of 15.0% established by the Brazilian Health Regulatory Agency (ANVISA) for flours and starches, indicating adequate stability and suitability for further processing. Moisture content is a critical parameter, as it can influence starch flowability, storage stability, and processing behavior (Zhang et al., 2018).

The amylose content of starch was of 31.55% ± 2.39, which is considered relatively high for wheat starch. Similar values have been reported by Baranzelli et al. (2019), ranging from 30.81 to 35.56%, while El Halal et al. (2019) reported a broader variation (22–35%) depending on the wheat cultivar. Such variability is strongly influenced by genetic factors, environmental conditions, and post-harvest handling, which affect starch biosynthesis and structure (Silveira et al., 2020; Wang et al., 2020).

From a structural and functional perspective, high-amylose content plays a crucial role in determining the physicochemical behavior of starch. Amylose molecules, due to their predominantly linear structure, are capable of forming intermolecular associations and entanglements, which are essential for fiber formation processes (Kong & Ziegler, 2012). In contrast, amylopectin, with its highly branched structure, introduces steric hindrance that limits chain interaction and reduces the ability to form continuous nanofibers (Cao et al., 2022).

Therefore, starches with higher amylose content are particularly advantageous for electrospinning applications, as they promote better chain entanglement, solution stability, and fiber integrity. This results in the formation of more uniform and mechanically resistant nanofibers, as reported by Cao et al. (2022). In this context, the relatively high-amylose content observed in the present study suggests a strong potential for the production of starch-based nanofibers with improved structural properties.

Characterization of Polymer Solutions

Electrical Conductivity and Rheological Properties

Table 1 presents the results regarding the electrical conductivity and rheological properties of wheat starch polymer solutions containing different concentrations of IPE.

The analysis of the presented values shows that the electrical conductivity (EC) of wheat starch solutions increases proportionally with the concentration of IPE, ranging from 2.69 mS/cm to 2.89 mS/cm, 3.14 mS/cm, and 3.45 mS/cm for nanofibers containing 0%, 5%, 10%, and 15% extract, respectively. This behavior can be attributed to the presence of conductive compounds in the extract, which, when incorporated into the starch matrix, enhance electrical conduction.

The conductivity of the solution enables the transfer of electrical charges, favoring the interaction between the

Table 1 Electrical conductivity and rheological measurements of wheat starch polymeric solutions with different concentrations of *I. paraguariensis* coproduct extract

Solutions	EC (mS/cm)	T_0 [Pa]	k [Pa.sn]	(n) [-]	R^2
0% IPE	$2.69 \pm 0.03^{d*}$	1.5075 ± 0.14^{a}	1.182 ± 0.04^{a}	0.7227 ± 0.01^{b}	0.9736
5% IPE	2.89 ± 0.09^{c}	0.1666 ± 0.01^{b}	1.491 ± 0.14^{a}	0.6526 ± 0.00^{d}	0.9731
10% IPE	3.14 ± 0.03^{b}	0.1008 ± 0.00^{b}	1.179 ± 0.16^{a}	0.7130 ± 0.01^{c}	0.9683
15% IPE	3.45 ± 0.03^{a}	0.1131 ± 0.02^{b}	1.259 ± 0.12^{a}	0.7246 ± 0.00^{a}	0.9758

EC, electrical conductivity; T_0, yield stress; *k*, consistency index; *n*, flow behavior index; R^2, determination coefficient. *Means followed by different letters in the same column indicate a significant difference between the data using the Tukey test ($p < 0.05$)

solution and the collector, in addition to promoting the stretching of the polymer jet, which directly depends on the solution's ability to transport these charges (Unnithan et al., 2015). When conductivity is higher, there is greater mobility of the ions in the solution and, under the application of the electric field, they tend to be more easily directed, resulting in greater jet elongation, which may reduce fiber diameter and prevent the presence of aggregates (Antunes et al., 2017; Pires et al., 2024b). The increase in conductivity did not impair the process, as the formation of stable and continuous jets was maintained. However, an increase in the average fiber diameter was observed, which may be explained by the rise in apparent viscosity or other process-related factors.

The rheological properties of the control solution (wheat starch only), as well as those of the solutions containing different concentrations of IPE (5, 10, and 15%, w/v), were evaluated through their flow behavior (viscosity as a function of shear rate, Fig. 1a) and storage (G') and loss (G'') moduli (Fig. 1b). For both samples, the data were well described using the Herschel-Bulkley model with coefficients of determination (R^2) (Table 1). When the IPE was added, the viscosity of the solution remained stable with a slight decrease (10% IPE) up to a certain point; however, at a concentration of 15% IPE, the behavior was similar to the control, which suggests that up to a certain concentration IPE addition is favorable, and beyond that, the solution tends to become more viscous due to the solutes present in the IPE extract. This behavior is explained by the flow behavior index (n) (Table 1), which presented values lower than one, indicating a non-Newtonian pseudoplastic behavior. A similar behavior was also observed by Santos et al. (2024a) when evaluating the viscosity of bean starch solutions containing geranium essential oil. Regarding the consistency index (k), no significant differences ($p < 0.05$) were observed among the samples, although a slight increasing trend was noted with higher concentrations of co-product extract, indicating greater resistance to flow.

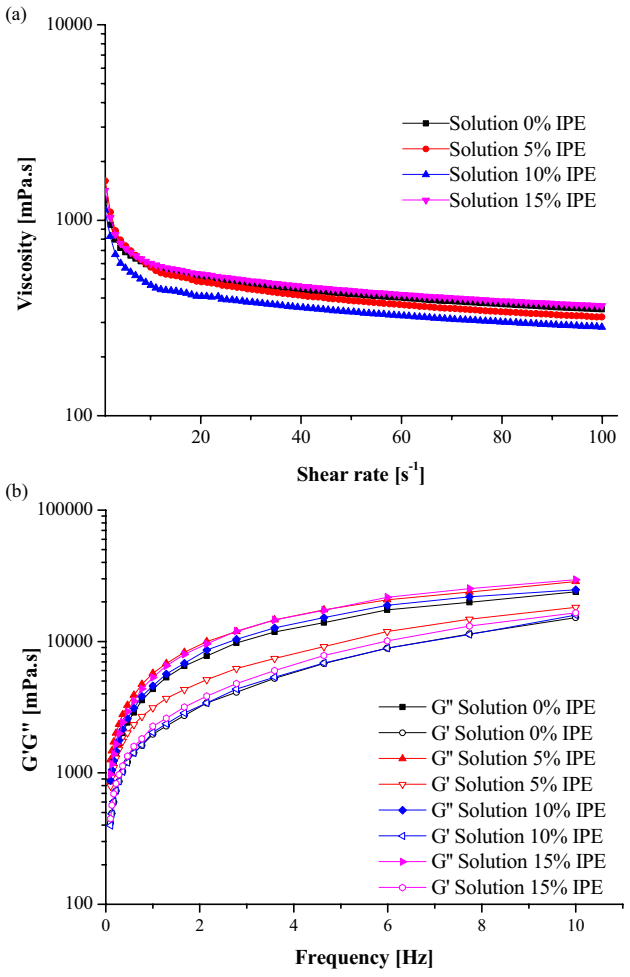


Fig. 1 Flow behavior (**a**) and storage (G') and loss (G'') (**b**) moduli of polymeric wheat starch solutions with different concentrations of IPE

The increase in solution concentration is directly associated with a rise in viscosity due to greater entanglement of polymer chains, which contributes to jet stabilization during fiber formation (Wang et al., 2016). Although the viscosity of the solutions increased, this increment was not sufficient to hinder the electrospinning process, but it did result in nanofibers with a larger average diameter. In highly viscous solutions, jet stretching becomes limited, leading not only to an increase in fiber diameter but also to the appearance of agglomerates known as beads (Wang et al., 2009).

The analysis of the storage (G') and loss (G'') moduli as a function of frequency (0–10 rad/s) of the polymeric solutions is presented in Fig. 1b. At all concentrations evaluated, the loss modulus (G'') remained higher than the storage modulus (G') throughout the entire frequency range, demonstrating the predominance of viscous over elastic behavior. This result is consistent with previous studies on aged corn starch solutions with different amylose contents and wheat starch nanoparticles, which report that systems with predominantly viscous behavior exhibit higher apparent viscosity values and larger hydrodynamic diameters (Herrera et al., 2017). Electrical conductivity, viscosity, and polymer concentration are key parameters in the electrospinning process, directly influencing fiber morphology (Rostamabadi et al., 2020; Santos et al., 2024a). In the present study, the increase in electrical conductivity with higher IPE concentrations indicates enhanced ionic mobility and charge transport capacity. Conversely, the rheological results demonstrated a pseudoplastic behavior ($n < 1$) and a slight increase in flow resistance at higher extract concentrations, suggesting greater molecular interactions within the system. While higher conductivity tends to intensify electrostatic forces and

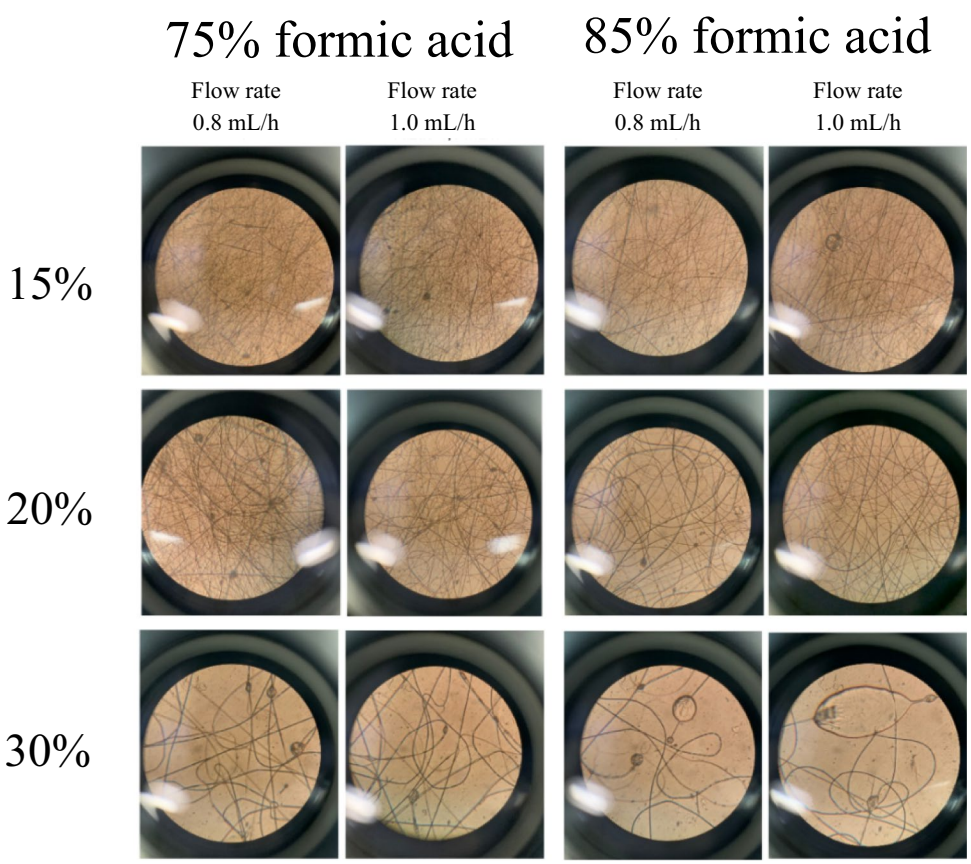


Fig. 2 Test polymeric solutions using different concentrations of wheat starch and formic acid

promote jet stretching, the concurrent increase in viscosity limits chain mobility and resists elongation. Thus, the electrospinning process is governed by the balance among these competing effects, and shifts in this balance directly influence jet stability and deformation behavior, impacting nanofiber formation.

Morphology and Size Distribution of the Nanofibers

The morphological evaluation of the nanofibers by optical microscopy (Figs. 2 and 3) demonstrated that starch concentration had a direct influence on the resulting structure. The formulation containing 15% starch produced finer, continuous, and more homogeneous nanofibers (Fig. 2), with a low incidence of defects such as beads and discontinuities. In contrast, higher concentrations (20 and 30%) of starch exhibited greater structural irregularity, possibly associated with increased solution viscosity, which may hinder jet stretching during electrospinning. It is important to note that, although parameters such as viscosity and electrical conductivity are known to be determinant in this process, these properties were not evaluated at this stage of the study. Regarding the processing conditions, it was observed that the higher formic acid concentration (85%) combined with a higher flow rate (1.0 mL/h) resulted in thicker, less uniform nanofibers with the presence of beads. Based on these results, the most suitable condition was defined as the use of 75% (v/v) formic acid, 15% (w/v) wheat starch, and a flow rate of 0.8 mL/h, as these conditions favored the formation of more homogeneous, continuous, and defect-free nanofibers.

In Fig. 3, it can be observed that the concentration of IPE added to the nanofiber-forming solution (15% w/v wheat starch) had a significant influence on the formation of continuous and uniform structures. As the extract concentration increased, a higher incidence of defects was observed, particularly at concentrations above 15% (w/w), and this effect was further intensified with increasing flow rate. Based on these results, and aiming to obtain continuous, homogeneous, and defect-free nanofibers, only the concentrations of 5%, 10%, and 15% (w/w) IPE were selected for the production of wheat starch nanofibers.

The morphology (a, c, e, and g) and size distribution (b, d, f, and h) of wheat starch nanofibers, both control and those containing IPE (0%, 5%, 10%, and 15%), are shown in Fig. 4. The electrospinning conditions led to the formation of homogeneous, cylindrical, continuous, and smooth nanofibers, free of agglomerates (“beads”). The incorporation of the extract influenced nanofibers’ morphology in a concentration-dependent manner. Although all formulations yielded continuous fibers, slight changes in fiber diameter distribution and uniformity were observed, particularly at higher extract concentrations.

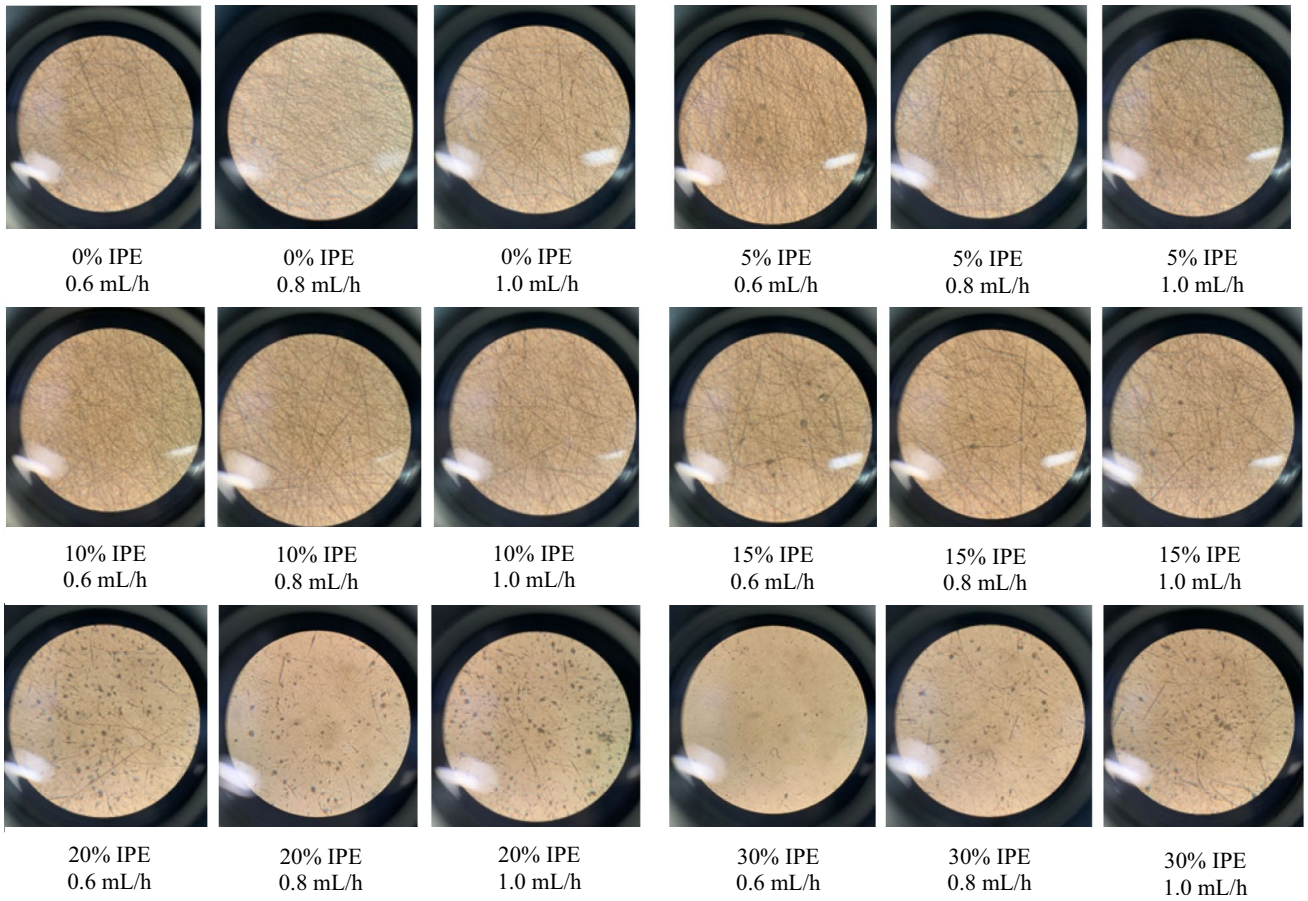


Fig. 3 Polymeric solutions of 15% wheat starch and incorporation of the lyophilized extract of the co-product of *I. paraguariensis* in different concentrations

These findings indicate that fiber formation was not compromised; however, morphological attributes were moderately affected, as reflected by the reduction in the average fiber diameter. The average fiber diameters showed a slight increase with the incorporation of the extract into the solutions. Pure wheat starch presented an average diameter of 195 ± 25 nm, while the addition of 5% co-product extract resulted in 218 ± 28 nm. At IPE concentrations of 10% (214 ± 32 nm) and 15% (204 ± 24 nm), a slight reduction in fibers' diameter was observed compared with the 5% treatment. Analysis of variance (ANOVA) indicated a significant difference ($p < 0.05$) between the 0% (195 nm) and 5% (218 nm) treatments, as well as between 0% (195 nm) and 10% (214 nm), confirming that the addition of the extract increased the nanofiber diameter. In general, low-viscosity solutions tend to produce nanofibers with smaller diameters (Fonseca et al., 2020a); however, in the present study, the opposite behavior was observed, in which the 5% IPE solution exhibited the lowest viscosity and the largest average nanofibers' diameter. This behavior may be associated with the presence of compounds from the IPE, which, although reducing the viscosity of the solution, also altered parameters such as electrical conductivity and surface tension. This combined effect may have limited jet stretching during electrospinning, resulting in nanofibers with larger diameters, even in the less viscous solution.

Encapsulation Efficiency

The encapsulation efficiency of wheat starch nanofibers containing extract from IPE was $90.8 \pm 6.24\%$, $68.2 \pm 11.8\%$, and $63.7 \pm 9.96\%$ for samples with 5%, 10%, and 15%, respectively, showing high efficiency at lower concentrations and a progressive reduction with increasing extract content. This behavior is similar to that reported by Fonseca et al. (2020b) in potato starch nanofibers, in which increasing the concentration of pinhão nut shell extract resulted in lower loading capacity (62–100%) when

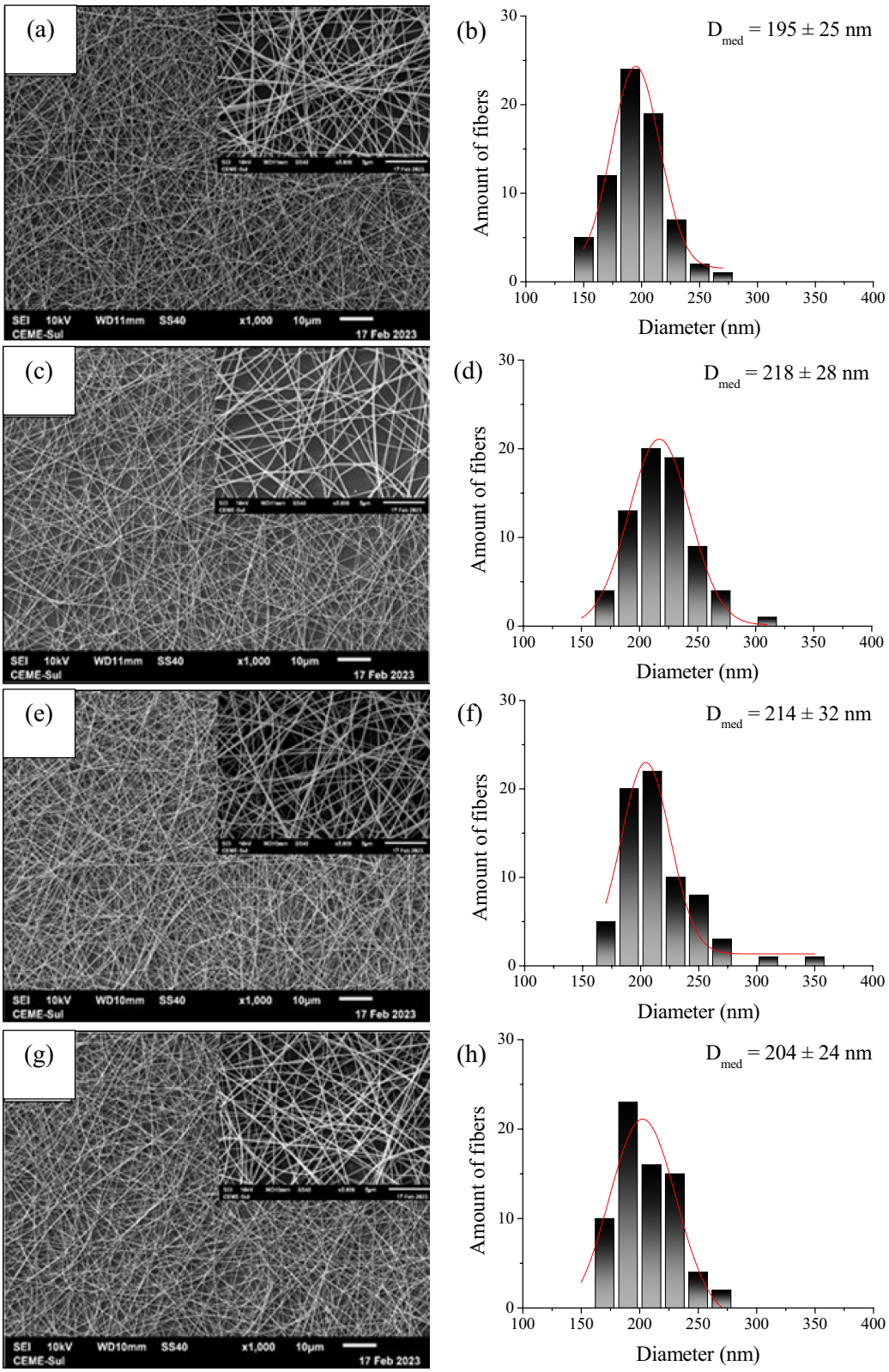


Fig. 4 Morphology and size distribution of nanofibers of wheat starch incorporated with different concentrations of IPE (0% (**a** and **b**), 5% (**c** and **d**), 10% (**e** and **f**), and 15% (**g** and **h**)), respectively

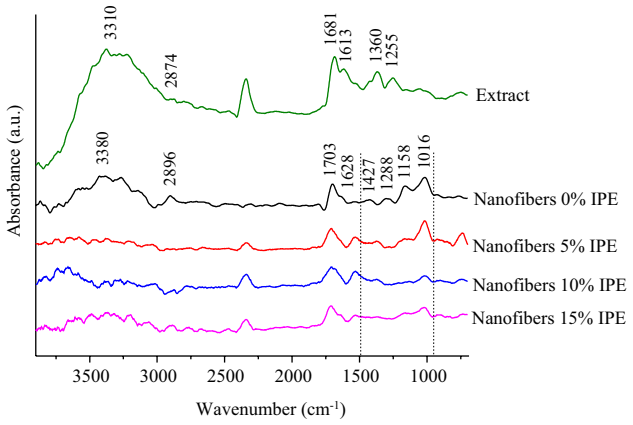


Fig. 5 Fourier transform infrared spectra of extract, and nanofibers of wheat starch at different concentrations of IPE

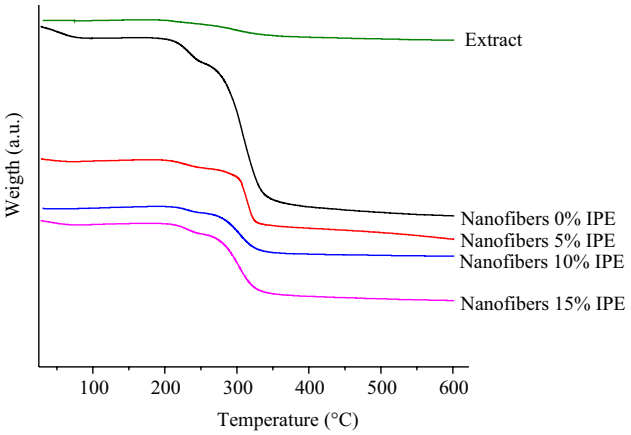


Fig. 6 Thermogravimetric analysis of the extract and nanofibers samples with different IPE concentrations (0%, 5%, 10%, and 15%)

incorporated at 0.5%, 1.0%, and 1.5% of extract. However, the authors observed that the highest encapsulation efficiency was achieved at the lowest extract concentration (0.5%), which is consistent with the results found in this study. A decreasing trend was also reported by Santos et al. (2023) (58.0–66.8%) when evaluating the encapsulation efficiency of zein nanofibers containing jambolan extract. In our study, wheat starch nanofibers containing the lowest concentration of IPE (5%) showed satisfactory matrix performance, in accordance with the 70% threshold suggested by Yun et al. (2021) as the minimum for industrial feasibility. Thus, the results demonstrate that wheat starch presents great potential as an encapsulating matrix, being able to efficiently retain the bioactive compounds from IPE at low concentrations. In contrast, higher extract concentrations led to an increase in structural irregularities. This behavior is consistent with the average fiber diameter results, in which nanofibers containing the lowest extract concentration (5%) showed higher encapsulation efficiency, possibly due to their larger diameter, which favors the incorporation and retention of bioactive compounds from IPE.

Functional Groups

The functional groups were identified by Fourier-transform infrared spectroscopy (FTIR). The lyophilized extract from the IPE showed characteristic bands of polyphenols (Fig. 5), with a band at 3310 cm^{-1} (νO–H overlapping νN–H) corresponding to hydroxyl groups present in compounds such as chlorogenic acid, saponins, xanthines, and others (Gullón et al., 2018). A band at 2874 cm^{-1} (νsC–H; νaC–H) was observed for aliphatic groups, along with one at 1661 cm^{-1} (νC = O) corresponding to the carbonyl group present in esters, amides, and xanthines, and another at 1613 cm^{-1} (νC = O) associated with carboxyl groups in acids and saponins. Finally, bands were observed at 1360 cm^{-1} (δsCH_3CO) and 1255 cm^{-1} (νasC–O–C; δC–O–H in-plane), attributed to cyclic ethers and other functional groups present in the compounds of *I. paraguariensis* (Gullón et al., 2018).

The 0% nanofibers showed bands at 3380 cm^{-1} (νO–H), which can be attributed to inter- and intramolecular hydroxyl groups between amylose chains, and at 2896 cm^{-1} (νsC–H; νaC–H) corresponding to the cyclic chain. Bands at 1703 cm^{-1} and 1628 cm^{-1} (δOH) were associated with hydrogen bonding in the amorphous region of the granules. A band at 1427 cm^{-1} (δsCH_2) corresponded to amylopectin, while 1288 cm^{-1} (δC–O–H) was related to out-of-plane bending, and 1158 cm^{-1} (νasC–O–C) was attributed to the α−1,4 glycosidic linkage. Additionally, chain-related bands were observed at 1016 cm^{-1} (νC–O). Similar bands were reported by Pires et al. (2022) in native potato starch. The 5%, 10%, and 15% nanofibers exhibited characteristic bands similar to those of the 0% fiber, where it can be observed that the fingerprint region ($1000 < cm^{-1} < 1500$) of the different nanofibers closely resembles that of the 0% fiber spectrum, suggesting effective encapsulation of the extract at all concentrations studied.

Thermal Properties

The thermal stability of IPE, as well as that of the nanofibers produced from wheat starch containing different extract concentrations (5, 10, and 15%, w/w), was evaluated by thermogravimetric analysis (TGA), and the results are presented in Fig. 6. The thermogram of IPE showed two main stages of mass loss, the first, around ~ 100 °C, associated with the evaporation of bound water, and the second, between ~ 200 and 380 °C, related to the degradation

of low-molecular-weight compounds and more complex structures, such as hemicellulose and pectins (Bruni et al., 2020).

Regarding the control nanofibers, three stages of mass loss were observed, the first, between ~ 40 and ~ 100 °C, attributed to the evaporation of water present in the material, the second, in the range of ~ 200 to 280 °C, related to the elimination of ester groups formed during the esterification reaction between formic acid and starch, and finally, the third stage, between ~ 310 and 410 °C, associated with the decomposition of the starch structure (Santos et al., 2024a, 2025).

For nanofibers containing different concentrations of IPE (5, 10, and 15%, w/w), the obtained thermograms were similar to that of the control nanofibers, showing three stages of mass loss, attributed respectively to the evaporation of bound water, the decomposition of groups formed during the esterification process, and finally the degradation of wheat starch. Regarding the IPE incorporated into the nanofibers, it is likely that interactions occurred between the extract constituents and the hydroxyl groups of starch, which may explain the absence of the mass loss stage observed for the pure extract (around ~ 200 °C). This behavior suggests that the degradation of the extract compounds occurred simultaneously with the decomposition of the starch matrix, at temperatures close to ~ 350 °C. This result suggests improved thermal stability of the nanofibers incorporated with the extract.

Contact Angle

The static contact angle (θ) of the solid–liquid interface was measured between the nanofiber membranes and ultrapure water. All nanofibers exhibited contact angles below 90°, specifically $\theta = 28.26 \pm 6.15°$, $\theta = 32.67 \pm 0.15°$, $\theta = 27.72 \pm 0.56°$, and $\theta = 27.24 \pm 2.91°$ for the nanofibers containing 0%, 5%, 10%, and 15% IPE, respectively, indicating hydrophilic surfaces according to the classification by Ahmad et al. (Ahmad & Kan, 2016) (Fig. 7). Initially, an increase in θ was observed when comparing the 0% and 5% nanofibers. This behavior may have occurred because wettability is influenced by the presence of polar and nonpolar groups on the nanofibers surface. The surface modification can be explained by the incorporation of the extract, which contains various compounds in its composition; however, the increase in contact angle suggests the presence of free polar groups on the nanofibers surface, indicating that the active sites of the 5% nanofibers were responsible for this behavior. In contrast, the 10% and 15% nanofibers showed a decrease in contact angle, confirming the occupation of more active sites and demonstrating that as the concentration of incorporated co-product increases, the fiber becomes progressively more hydrophilic, enhancing its wettability properties.

These results are consistent with those reported by Cruz et al. (2023), and Santos et al. (2023), who observed a decrease in contact angle with increasing concentrations of encapsulated red onion peel and jambolan extracts in yellow and white sweet potato starch and zein matrices, respectively. This behavior can be explained by the hydrophilic nature of phenolic extracts, which exhibit high water solubility, thereby promoting a reduction in contact angle.

Table 2 Antioxidant activities against $ABTS^{\bullet+}$ and DPPH radicals of IPE, and incorporated into wheat starch nanofibers

Samples	$ABTS^{\bullet+}$ (%)	DPPH (%)
Nanofibers 0% IPE	nd	6.57 ± 0.43^{d}
Nanofibers 5% IPE	47.01 ± 6.61^{c}	22.70 ± 0.30^{c}
Nanofibers 10% IPE	60.48 ± 8.04^{b}	33.13 ± 0.36^{a}
Nanofibers 15% IPE	97.83 ± 0.53^{a}	24.91 ± 1.16^{b}

Nd, not detected. Means followed by different letters in the same column indicate a significant difference between the data using the Tukey test ($p < 0.05$)

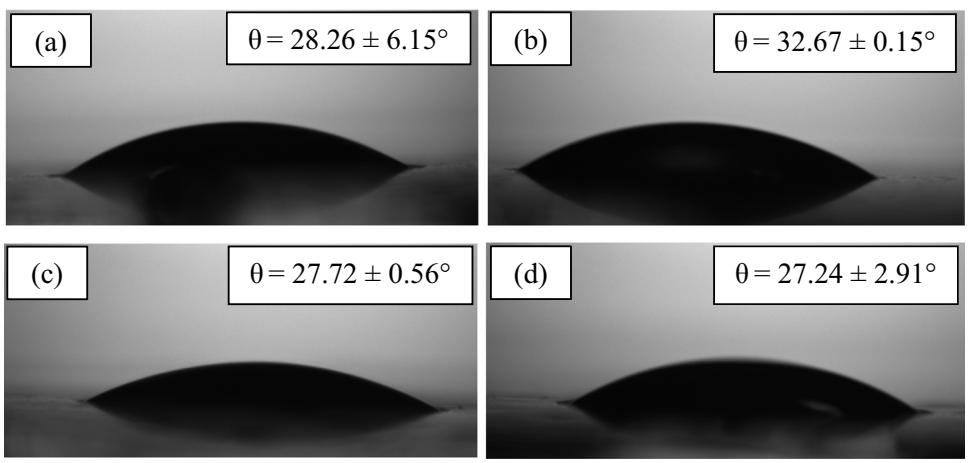


Fig. 7 Solid–liquid interface angle of nanofibers samples containing different concentrations of IPE (0% (**a**), 5% (**b**), 10% (**c**), and 15% (**d**))

Furthermore, the contact angle is also influenced by the capillary effect of the membrane and varies according to surface roughness, morphology, nanofibers diameter, and porosity (Correia et al., 2015), factors that can modify the membrane's surface tension and consequently affect its hydrophilicity and wettability.

Antioxidant Activity

Table 2 presents the results of the antioxidant activities of the IPE, encapsulated in wheat starch nanofibers, against the $ABTS^{\bullet+}$ and DPPH radicals.

The control nanofibers (0%) showed no antioxidant activity against the $ABTS^{\bullet+}$ radical and only low activity against the DPPH radical (6.57%), indicating that wheat starch nanofibers alone do not possess relevant antioxidant activity. Antioxidant activity increased significantly when the extract was incorporated into the wheat starch nanofibers, and the higher the amount of incorporated extract, the greater the observed antioxidant activity. The 5%, 10%, and 15% nanofibers showed a significant increase ($p > 0.05$) in $ABTS^{\bullet+}$ radical inhibition, with the 15% fiber exhibiting the highest activity (97.83%). However, for the DPPH radical, the 5% and 10% nanofibers showed an increase in activity, while the 15% nanofibers displayed a decrease. This behavior may be explained by the fact that the 5% and 10% nanofibers contain intermediate concentrations of IPE, in which the antioxidant compounds may be more accessible and more evenly distributed within the nanofibers, resulting in higher antioxidant activity as measured by the DPPH assay. Moreover, the DPPH radical is a specific chemical species that may react differently with the antioxidant compounds of the extract depending on their concentration, which could explain the variations observed in the antioxidant activity of the nanofibers against this radical. These results indicate that wheat starch nanofibers exhibit a greater inhibition capacity against the $ABTS^{\bullet+}$ radical compared to the DPPH radical. Furthermore, the incorporation of the co-product into electrospun wheat starch nanofibers may partially protect the functional properties of the phenolic compounds.

Studies such as that of Fonseca et al. (2020a) demonstrated that the incorporation of thyme essential oil into sweet potato starch nanofibers also resulted in lower DPPH inhibition capacity. In another study using white and yellow sweet potato starches to encapsulate flavonoids from red onion peel, the authors observed a significant increase in antioxidant activity with higher concentrations of the lyophilized compound (Cruz et al., 2023). However, no studies have been found using wheat starch nanofibers for the encapsulation of bioactive compounds. However, in the lyophilized free extract, a lower inhibition capacity against the $ABTS^{\bullet+}$ radical was observed, which may be related to the complexation of compounds, leading to an increased activity when incorporated into the nanofibers. In samples of dried commercial yerba mate leaves, inhibition levels of up to 94% have been reported (Akbarmehr et al., 2023). When incorporating pinhão coat extract into potato starch nanofibers, an inhibition of 28% was obtained, which is lower than that found in the present study (Fonseca et al., 2020b). Similarly,

Table 3 In vitro release of chlorogenic acids in hydrophilic (10% ethanol) and lipophilic (50% ethanol), and thermal resistance at temperatures of 120 °C of wheat starch nanofibers with different concentrations of IPE

Release with 10% ethanol (%, w/w)						
Sample	5-CQA	3-CQA	4-CQA	3.4-DQA	3.5-DQA	4.5-DQA
Nanofibers 5% IPE	59.73 ± 3.91^{b}	44.72 ± 2.94^{b}	41.14 ± 2.46^{b}	nd	nd	nd
Nanofibers 10% IPE	67.00 ± 2.17^{a}	52.06 ± 3.07^{a}	53.69 ± 3.48^{a}	nd	nd	nd
Nanofibers 15% IPE	70.72 ± 0.66^{a}	56.61 ± 1.91^{a}	58.28 ± 0.98^{a}	nd	nd	nd
Release with 50% ethanol (%, w/w)						
Sample	5-CQA	3-CQA	4-CQA	3.4-DQA	3.5-DQA	4.5-DQA
Nanofibers 5% IPE	52.01 ± 1.94^{a}	59.77 ± 2.27^{a}	40.01 ± 4.51^{a}	27.41 ± 1.63^{c}	70.04 ± 4.64b	53.82 ± 3.38^{b}
Nanofibers 10% IPE	52.58 ± 2.18^{a}	62.45 ± 2.06^{a}	38.81 ± 4.83^{a}	35.43 ± 1.41^{b}	78.38 ± 4.33ab	58.23 ± 2.78^{ab}
Nanofibers 15% IPE	56.05 ± 1.89^{a}	63.68 ± 1.46^{a}	39.34 ± 1.64^{a}	40.47 ± 0.39^{a}	82.71 ± 0.64a	61.17 ± 1.44^{a}
Thermal resistance (%, w/w)						
Sample	5-CQA	3-CQA	4-CQA	3.4-DQA	3.5-DQA	4.5-DQA
Extract	25.14 ± 3.87^{a}	27.64 ± 4.30^{c}	31.61 ± 5.16^{c}	48.02 ± 4.16^{a}	21.96 ± 5.03^{c}	34.58 ± 8.50^{c}
Nanofibers 5% IPE	80.14 ± 6.89^{b}	77.83 ± 13.01^{a}	86.01 ± 0.09^{a}	nd	58.16 ± 2.10^{a}	100.00 ± 2.63^{a}
Nanofibers 10% IPE	73.51 ± 7.49^{b}	88.01 ± 10.46^{a}	86.22 ± 4.41^{a}	nd	32.85 ± 4.97^{b}	56.23 ± 13.80^{b}
Nanofibers 15% IPE	63.72 ± 10.30^{b}	50.62 ± 5.52^{b}	52.46 ± 3.33^{b}	26.80 ± 2.14^{b}	6.95 ± 0.95^{d}	3.59 ± 0.06^{d}

Means ± standard deviation. *5-CQA*, 5-caffeoylquinic; *3-CQA*, 3-caffeoylquinic; *4-CQA*, 4-caffeoylquinic; *3.4-DQA*, 3.4-dicaffeoylquinic; *3.5-DQA*, 3.5-dicaffeoylquinic; *4.5-DQA*, 4.5-dicaffeoylquinic. *nd*, not detection. Different letters indicate a statistically significant difference between the columns ($p < 0.05$)

Pires et al. (2022) observed a gradual increase in radical scavenging activity, reaching up to 45%, when curcumin was incorporated at different concentrations (0.5%, 0.75%, and 1%) into native potato starch.

According to Cruz et al. (2023), antioxidants can delay or inhibit the oxidation of foods; however, they may degrade when exposed to environmental conditions. The encapsulation of phenolic compounds from the *I. paraguariensis* co-product is important for maintaining their stability, minimizing degradation caused by environmental factors such as light, heat, and temperature.

In Vitro Release Simulation

The simulated release of chlorogenic acids from *I. paraguariensis* extract encapsulated in wheat starch nanofibers, under hydrophilic (10% ethanol) and lipophilic (50% ethanol) conditions, is presented in Table 3. According to Commission Regulation (EU) (2011), a 10% ethanol solution represents hydrophilic conditions. Under these conditions, the release of caffeoylquinic acids (5-CQA, 3-CQA, and 4-CQA) increased with the IPE concentration, reaching a maximum release of 70.72% for 5-CQA in nanofibers containing 15% (w/w) extract.

In contrast, a 50% ethanol solution, which simulates lipophilic conditions (Commission Regulation (EU), 2011), promoted a different release behavior. In this medium, both caffeoylquinic acids (5-CQA, 3-CQA, and 4-CQA) and dicaffeoylquinic acids (3,4-DQA, 3,5-DQA, and 4,5-DQA) were released from the nanofibers. Among these compounds, 3,5-DQA showed the highest release, reaching 82.71% in nanofibers containing 15% (w/w) IPE.

The release of chlorogenic acids present in IPE encapsulated in wheat starch nanofibers should be tailored according to the intended application. Under conditions simulating less aggressive media (such as 10% ethanol), a slower release is desirable, as it promotes the protection of phenolic compounds against degradation, allowing for gradual availability while maintaining their stability and functionality over time (Fonseca et al., 2020b). This behavior is particularly relevant for applications in active packaging, where the goal is to extend food shelf life through the continuous antioxidant activity of these compounds (Cruz et al., 2023).

On the other hand, under more aggressive conditions (such as 50% ethanol), a faster release of chlorogenic acids may occur and, in certain cases, is also desirable, especially for foods with shorter shelf life, where immediate antioxidant and antimicrobial action is required, such as minimally processed vegetables (Cruz et al., 2023). Therefore, the release profile of encapsulated bioactive compounds can be adjusted according to the type of food and storage conditions, enabling the application of these nanofibers in both lipid and aqueous systems.

Thermal Resistance

Chlorogenic acids present in IPE, both in free form and encapsulated in wheat starch nanofibers, exhibited thermal resistance when subjected to 120 ºC for 1 h (Table 3). However, the non-encapsulated extract showed lower stability, with thermal resistance values below 48%, which was expected due to the higher thermal sensitivity of phenolic compounds in their free form (Meinhart et al., 2019). In contrast, nanofibers containing different concentrations of IPE showed higher thermal resistance, with values exceeding 58% for most of the chlorogenic acids analyzed, with the nanofibers containing 5% IPE exhibiting the highest stability. However, for the compounds 3,5-DQA and 4,5-DQA in nanofibers with the highest extract concentration (15%; w/w),

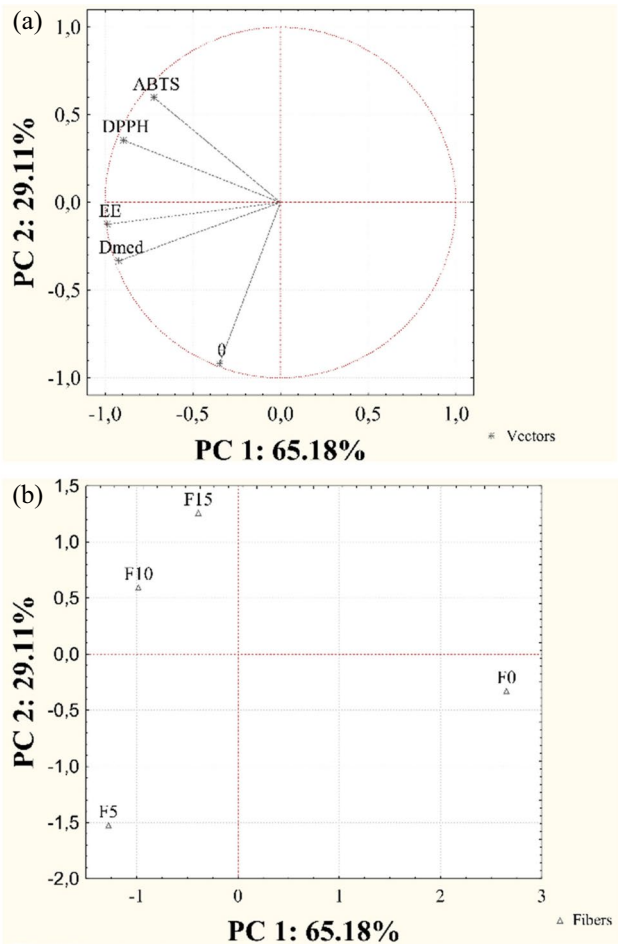


Fig. 8 Principal component analysis: variable cloud (**a**) and point cloud (**b**)

lower thermal resistance was observed, possibly related to the greater release of these compounds in a 50% ethanol simulant medium (Table 3). Overall, the results indicate that encapsulation in wheat starch nanofibers produced by electrospinning significantly improved the thermal stability of chlorogenic acids, likely due to interactions between the extract constituents and the polymer matrix, which enhance their protection under elevated temperature conditions.

Principal Component Analysis (PCA)

The PCA performed on the dataset of the nanofibers (D_{med}, EE, θ, DPPH, and $ABTS^{\bullet+}$) indicated that the increase in extract concentration significantly affected the fiber characteristics. This was evidenced by the strong linear contribution and the magnitude of the vectors positioned close to or overlapping the unit circle on the factorial plane in the variable cloud (Fig. 8a).

Three distinct groups were formed in the score plot (Fig. 8b), with the nanofibers containing 10% and 15% IPE (F10 and F15, respectively) clustered together, indicating that, for the variables studied, the effects of these concentrations were similar. These nanofibers were distinct from the control nanofibers (F0) and those with 5% IPE (F5), suggesting that the effect of the extract in modifying the fiber characteristics to produce distinct materials occurs at higher concentrations.

The antioxidant activity in stabilizing the $ABTS^{\bullet+}$ and DPPH radicals was higher in the nanofibers containing 10% and 15% of IPE as indicated by their position in the same quadrant of the factorial plane. The vectors θ, D_{med}, and EE were associated with the nanofibers containing 5% of IPE, which showed higher values for these respective variables. These findings are consistent with those discussed in the previous sections.

Conclusion

Wheat starch nanofibers containing *Ilex paraguariensis* co-product extract (IPE) were successfully produced by electrospinning, exhibiting a smooth, homogeneous, and defect-free morphology. The incorporation of the extract influenced solution properties, such as viscosity and electrical conductivity, resulting in variations in fiber diameter. The highest encapsulation efficiency (90.8%) was achieved at 5% extract concentration, with a decrease observed at higher concentrations.

Encapsulation affected the antioxidant activity depending on the radical evaluated. An increase in $ABTS^{\bullet+}$ radical scavenging activity was observed after incorporation into the nanofibers, while the activity against the DPPH radical was partially preserved. Thermal analysis demonstrated greater stability of the encapsulated extract compared to the free extract, and FTIR results confirmed its incorporation into the starch matrix. Additionally, the presence of the extract increased the wettability of the nanofibers, making them more hydrophilic. The nanofibers exhibited a controlled release profile of chlorogenic acids, with slower release in hydrophilic media and faster release under lipophilic conditions, indicating potential for different food applications. Furthermore, encapsulation significantly enhanced the thermal resistance of the bioactive compounds, highlighting the protective effect of the polymeric matrix.

Overall, the results demonstrate that IPE is a promising source of natural antioxidants, while wheat starch stands out as an efficient and sustainable polymeric matrix for electrospinning and encapsulation. This study also contributes to the principles of the circular economy by valorizing yerba mate residues. Future studies should investigate the application of these nanofibers in real food systems, aiming to explore their technological and functional potential to improve food quality and stability.

Acknowledgements We also thank the Southern Electron Microscopy Center (CEME-SUL) at FURG.

Author Contributions F.N.S., Y.V.B.M., A.G.L.R., L.V.C. and I.H.L.C.: Conceptualization, Data curation, Formal analysis, Investigation, Methodology, Software, Roles/Writing—original draft, Writing – review & editing. T.R.R.V. and T.C.A.S.: Conceptualization, Data curation, Formal analysis, Investigation, Software. H.C.S.: Visualization, Formal analysis, Methodology. E.R.Z.: Conceptualization, Project administration, Supervision, Validation, Visualization, Writing—review & editing. A.D.M.: Conceptualization, Funding acquisition, Project administration, Resources, Supervision, Validation, Visualization, Writing—review & editing.

Funding The Article Processing Charge (APC) for the publication of this research was funded by the Coordenação de Aperfeiçoamento de Pessoal de Nível Superior - Brasil (CAPES) (ROR identifier: 00x0ma614). The publication of this article received funding from the Conselho Nacional de Desenvolvimento Científico e Tecnológico (CNPq), Coordenação de Aperfeiçoamento de Pessoal de Nível Superior (CAPES), code: 001, and Fundação de Amparo à Pesquisa do Estado do Rio Grande do Sul (FAPERGS), Brazil, and was partially supported by PPGCTA/UFPel.

Data Availability All relevant data are within the manuscript and available from the corresponding author upon request.

Declarations

Competing Interests The authors declare no competing interests.

Open Access This article is licensed under a Creative Commons Attribution 4.0 International License, which permits use, sharing, adaptation, distribution and reproduction in any medium or format, as long as you give appropriate credit to the original author(s) and the source, provide a link to the Creative Commons licence, and indicate if changes were made. The images or other third party material in this article are included in the article's Creative Commons licence, unless indicated otherwise in a credit line to the material. If material is not included in

the article's Creative Commons licence and your intended use is not permitted by statutory regulation or exceeds the permitted use, you will need to obtain permission directly from the copyright holder. To view a copy of this licence, visit http://creativecommons.org/licenses/by/4.0/.

References

Ahmad, I., & Kan, C. W. (2016). A review on development and applications of bio-inspired superhydrophobic textiles. *Materials*. https://doi.org/10.3390/ma9110892

Akbarmehr, A., Peighambardoust, S. H., Soltanzadeh, M., Jafari, S. M., & Sarabandi, K. (2023). Microencapsulation of Yerba mate extract: The efficacy of polysaccharide/protein hydrocolloids on physical, microstructural, functional, and antioxidant properties. *International Journal of Biological Macromolecules, 234*, Article 123678. https://doi.org/10.1016/j.ijbiomac.2023.123678

Ali, N., Rashid, S., Nafees, S., Hasan, S. K., Shahid, A., Majed, F., & Sultana, S. (2017). Protective effect of Chlorogenic acid against methotrexate induced oxidative stress, inflammation and apoptosis in rat liver: An experimental approach. *Chemico-Biological Interactions, 272*, 80–91. https://doi.org/10.1016/j.cbi.2017.05.002

Antunes, M. D., Dannenberg, G. S., Fiorentini, Â. M., Pinto, V. Z., Lim, L.-T., Zavareze, E. R., & Dias, A. R. G. (2017). Antimicrobial electrospun ultrafine nanofibers from zein containing eucalyptus essential oil/cyclodextrin inclusion complex. *International Journal of Biological Macromolecules, 104*, 874–882. https://doi.org/10.1016/j.ijbiomac.2017.06.095

AOAC. (2000). Association of Official Analytical Chemists. Official Methods of Analysis, 17th ed.; Association of Official Analytical Chemists: Washington, DC, USA, 490–510.

Ashraf, R., Sofi, H. S., Malik, A., Beigh, M. A., Hamid, R., & Sheikh, F. A. (2019). Recent trends in the fabrication of starch nanonanofibers: Electrospinning and non-electrospinning routes and their applications in biotechnology. *Applied Biochemistry and Biotechnology, 187*(1), 47–74. https://doi.org/10.1007/s12010-018-2797-0

Baranzelli, J., Kringel, D. H., Mallmann, J. F., Bock, E., El Halal, S. L. M., Prietto, L., Zavareze, E. R., Miranda, M. Z., & Dias, A. R. G. (2019). Impact of wheat (*Triticum aestivum* L.) germination process on starch properties for application in films. *Starch/Staerke, 71*(7–8), 1–8. https://doi.org/10.1002/star.201800262

Bruni, G. P., Acunha, T. S., Oliveira, J. P., Fonseca, L. M., Silva, F. T., Guimarães, V. M., & Zavareze, E. R. (2020). Electrospun protein nanofibers loaded with Yerba mate extract for bioactive release in food packaging. *Journal of the Science of Food and Agriculture, 100*(8), 3341–3350. https://doi.org/10.1002/jsfa.10366

Cao, P., Wu, G., Yao, Z., Wang, Z., Li, E., Yu, S., Liu, Q., Gilbert, R. G., & Li, S. (2022). Effects of amylose and amylopectin molecular structures on starch electrospinning. *Carbohydrate Polymers, 296*, Article 119959. https://doi.org/10.1016/j.carbpol.2022.119959

European Commission. (2011). Commission Regulation (EU) No 10/2011 of 14 January 2011 on plastic materials and articles intended to come into contact with food. Official Journal of the European Union L 12/1, 15-1-2011.

Correia, D. M., Ribeiro, C., Sencadas, V., Botelho, G., Carabineiro, S. A. C., Ribelles, J. L. G., & Lanceros-Méndez, S. (2015). Influence of oxygen plasma treatment parameters on poly(vinylidene fluoride) electrospun fiber mats wettability. *Progress in Organic Coatings, 85*, 151–158. https://doi.org/10.1016/j.porgcoat.2015.03.019

Cruz, E. P., Jansen, E. T., Fonseca, L. M., Hackbart, H. C. S., Siebeneichler, T. J., Pires, J. B., Gandra, E. A., Rombaldi, C. V., Zavareze, E. R., & Dias, A. R. G. (2023). Red onion skin extract rich in flavonoids encapsulated in ultrafine nanofibers of sweet potato starch by electrospinning. *Food Chemistry, 406*, Article 134954. https://doi.org/10.1016/j.foodchem.2022.134954

El Halal, S. L. M., Kringel, D. H., Zavareze, E., & Dias, A. R. G. (2019). Methods for extracting cereal starches from different sources: A review. *Starch/Staerke, 71*(11–12), 1–14. https://doi.org/10.1002/star.201900128

Etxabide, A., Akbarinejad, A., Chan, E. W. C., Guerrero, P., de la Caba, K., Travas-Sejdic, J., & Kilmartin, P. A. (2022). Effect of gelatin concentration, ribose and glycerol additions on the electrospinning process and physicochemical properties of gelatin nanofibers. *European Polymer Journal, 180*, Article 111597. https://doi.org/10.1016/j.eurpolymj.2022.111597

Filip, E., Woronko, K., Stępień, E., & Czarniecka, N. (2023). An overview of factors affecting the functional quality of common wheat (*Triticum aestivum* L.). *International Journal of Molecular Sciences*. https://doi.org/10.3390/ijms24087524

Fonseca, L. M., Cruxen, C. E. S., Bruni, G. P., Fiorentini, Â. M., Zavareze, E. R., Lim, L. T., & Dias, A. R. G. (2019). Development of antimicrobial and antioxidant electrospun soluble potato starch nanonanofibers loaded with carvacrol. *International Journal of Biological Macromolecules, 139*, 1182–1190. https://doi.org/10.1016/j.ijbiomac.2019.08.096

Fonseca, L. M., Oliveira, J. P., Crizel, R. L., Silva, F. T., Zavareze, E. R., & Borges, C. D. (2020b). Electrospun starch nanofibers loaded with Pinhão (*Araucaria angustifolia*) coat extract rich in phenolic compounds. *Food Biophysics, 15*(3), 355–367. https://doi.org/10.1007/s11483-020-09629-9

Fonseca, L. M., Radünz, M., Hackbart, H. C. S., Silva, F. T., Camargo, T. M., Bruni, G. P., Monks, J. L. F., Zavareze, E. R., & Dias, A. R. G. (2020a). Electrospun potato starch nanofibers for thyme essential oil encapsulation: Antioxidant activity and thermal resistance. *Journal of the Science of Food and Agriculture, 100*(11), 4263–4271. https://doi.org/10.1002/jsfa.10468

Fonseca, L. M., Santos, F. N., Pires, J. B., Cruz, E. P., Pacheco, C. O., Diaz, P. S., Dias, A. R. G., & Zavareze, E. R. (2025). Electrospun nanofibers from esterified starch of tubers: Effect of concentration and source of starch on nanofibers performance. *Starch/Stärke, 77*(8), 1–14. https://doi.org/10.1002/star.202400150

Garcia-Lazaro, R. S., Lamdan, H., Caligiuri, L. G., Lorenzo, N., Berengeno, A. L., Ortega, H. H., Alonso, D. F., & Farina, H. G. (2020). In vitro and in vivo antitumor activity of yerba mate extract in colon cancer models. *Journal of Food Science, 85*(7), 2186–2197. https://doi.org/10.1111/1750-3841.15169

Godoy, R. C. B., Deliza, R., Gheno, L. B., Licodiedoff, S., Frizon, C. N. T., Ribani, R. H., & Santos, G. G. (2013). Consumer perceptions, attitudes and acceptance of new and traditional mate tea products. *Food Research International, 53*(2), 801–807. https://doi.org/10.1016/j.foodres.2013.02.054

Gullón, B., Eibes, G., Moreira, M. T., Herrera, R., Labidi, J., & Gullón, P. (2018). Yerba mate waste: A sustainable resource of antioxidant compounds. *Industrial Crops and Products, 113*, 398–405. https://doi.org/10.1016/j.indcrop.2018.01.064

Herrera, M. P., Vasanthan, T., & Chen, L. (2017). Rheology of starch nanoparticles as influenced by particle size, concentration and temperature. *Food Hydrocolloids, 66*, 237–245. https://doi.org/10.1016/j.foodhyd.2016.11.026

Jaramillo, C. M., Gutiérrez, T. J., Goyanes, S., Bernal, C., & Famá, L. (2016). Biodegradability and plasticizing effect of yerba mate extract on cassava starch edible films. *Carbohydrate Polymers, 151*, 150–159. https://doi.org/10.1016/j.carbpol.2016.05.025

Kim, H. H., Kim, M. J., Ryu, S. J., Ki, C. S., & Park, Y. H. (2016). Effect of fiber diameter on surface morphology, mechanical property, and cell behavior of electrospun poly(ε-caprolactone) mat. *Nanofibers and Polymers, 17*(7), 1033–1042. https://doi.org/10.1007/s12221-016-6350-x

Kong, L., & Ziegler, G. R. (2012). Role of molecular entanglements in starch fiber formation by electrospinning. *Biomacromolecules, 13*(8), 2247–2253. https://doi.org/10.1021/bm300396j

Kungel, P. T. A. N., Correa, V. G., Corrêa, R. C. G., Peralta, R. A., Soković, M., Calhelha, R. C., Bracht, A., Ferreira, I. C. F. R., & Peralta, R. M. (2018). Antioxidant and antimicrobial activities of a purified polysaccharide from yerba mate (*Ilex paraguariensis*). *International Journal of Biological Macromolecules, 114*, 1161–1167. https://doi.org/10.1016/j.ijbiomac.2018.04.020

Lim, L. T. (2020). *Electrospinning and electrospraying technologies for food and packaging applications*. Ultrafine Materials, High Performance Nanofibers and Wearables. Elsevier Ltd. https://doi.org/10.1016/B978-0-12-819611-3.00007-8

Lim, L.-T., Mendes, A. C., Chronakis, I. S. (2019). Electrospinning and electrospraying technologies for food applications. *In Advances in Food and Nutrition Research* (1st ed., Vol. 88). Elsevier Inc. https://doi.org/10.1016/bs.afnr.2019.02.005

Lorini, A., Damin, F. M., de Oliveira, D. N., Crizel, R. L., Godoy, H. T., Galli, V., & Meinhart, A. D. (2021). Characterization and quantification of bioactive compounds from *Ilex paraguariensis* residue by HPLC-ESI-QTOF-MS from plants cultivated under different cultivation systems. *Journal of Food Science, 86*(5), 1599–1619. https://doi.org/10.1111/1750-3841.15694

Meinhart, A. D., Damin, F. M., Caldeirão, L., de Jesus Filho, M., Silva, L. C., Constatn, L. S., Filho, J. T., Wagner, R., & Godoy, H. T. (2019). Chlorogenic and caffeic acids in 64 fruits consumed in Brazil. *Food Chemistry, 286*(5), 51–63. https://doi.org/10.1016/j.foodchem.2019.02.004

Meinhart, A. D., Damin, F. M., Caldeirão, L., Silveira, T. F. F., Filho, J. T., & Godoy, H. T. (2017). Chlorogenic acid isomer contents in 100 plants commercialized in Brazil. *Food Research International, 99*, 522–530. https://doi.org/10.1016/j.foodres.2017.06.017

Mendes, A. C., Stephansen, K., & Chronakis, I. S. (2017). Electrospinning of food proteins and polysaccharides. *Food Hydrocolloids, 68*, 53–68. https://doi.org/10.1016/j.foodhyd.2016.10.022

Mesquita, M., Santos, E., Kassuya, C. A., & Salvador, M. J. (2021). Chimarrão, terere and mate-tea in legitimate technology modes of preparation and consume: A comparative study of chemical composition, antioxidant, anti-inflammatory and anti-anxiety properties of the mostly consumed beverages of *Ilex paraguariensis* St. H. *Journal of Ethnopharmacology, 279*, Article 114401. https://doi.org/10.1016/j.jep.2021.114401

Oliveira, J. P., Bruni, G. P., Fonseca, L. M., Silva, F. T., Rocha, J. C., & Zavareze, E. R. (2020). Characterization of aerogels as bioactive delivery vehicles produced through the valorization of yerba-mate (*Illex paraguariensis*). *Food Hydrocolloids, 107*, Article 105931. https://doi.org/10.1016/j.foodhyd.2020.105931

Pagliosa, C. M., Vieira, M. A., Podestá, R., Maraschin, M., Zeni, A. L. B., Amante, E. R., & Amboni, R. D. M. C. (2010). Methylxanthines, phenolic composition, and antioxidant activity of bark from residues from mate tree harvesting (*Ilex paraguariensis* A. St. Hil.). *Food Chemistry, 122*(1), 173–178. https://doi.org/10.1016/j.foodchem.2010.02.040

Paim, B. T., Jansen-Alves, C., Rosas, A. L. G., Sousa, T. C. A., Massaut, Y. V. B., Alves, V., Santos, G. H. F., Deon, V. G., Pinto, V. Z., & Meinhart, A. D. (2024). Does the encapsulation of chlorogenic acids from *Ilex paraguariensis* co-product by spray-drying increase their stability? *Food Biophysics, 19*(2), 386–399. https://doi.org/10.1007/s11483-024-09830-0

Pires, J. B., Fonseca, L. M., Siebeneichler, T. J., Crizel, R. L., Santos, F. N., Hackbart, H. C. S., Kringel, D. H., Meinhart, A. D., Zavareze, E. R., & Dias, A. R. G. (2022). Curcumin encapsulation in capsules and fibers of potato starch by electrospraying and electrospinning: Thermal resistance and antioxidant activity. *Food Research International, 162*, Article 112111. https://doi.org/10.1016/j.foodres.2022.112111

Pires, J. B., Santos, F. N., Costa, I. H. L., Kringel, D. H., Zavareze, E. R., & Dias, A. R. G. (2023). Essential oil encapsulation by electrospinning and electrospraying using food proteins: A review. *Food Research International, 70*, Article 112970. https://doi.org/10.1016/j.foodres.2023.112970

Pires, J. B., Santos, F. N., Cruz, E. P., Fonseca, L. M., Pacheco, C. O., Rosa, B. N., Santana, L. R., Pereira, C. M. P., Carreno, N. L. V., Diaz, P. S., Zavareze, E. R., & Dias, A. R. G. (2024a). Cassava, corn, wheat, and sweet potato native starches: A promising biopolymer in the production of capsules by electrospraying. *International Journal of Biological Macromolecules, 281*, Article 136436. https://doi.org/10.1016/j.ijbiomac.2024a.136436

Pires, J. B., Santos, F. N., Cruz, E. P., Fonseca, L. M., Siebeneichler, T. J., Lemos, G. S., Gandra, E. A., Zavareze, E. R., & Dias, A. R. G. (2024b). Starch extraction from avocado by-product and its use for encapsulation of ginger essential oil by electrospinning. *International Journal of Biological Macromolecules*. https://doi.org/10.1016/j.ijbiomac.2023.127617

Rostamabadi, H., Assadpour, E., Tabarestani, H. S., Falsafi, S. R., & Jafari, S. M. (2020). Electrospinning approach for nanoencapsulation of bioactive compounds; recent advances and innovations. *Trends in Food Science and Technology, 100*, 190–209. https://doi.org/10.1016/j.tifs.2020.04.012

Santiano, F. E., Fernández, M. Á., Espino, M., Zyla, L. E., Rey, L., Gómez, S. E., Bruna, F. A., Pistone-Creydt, V., Pietrobon, E., Pérez Elizalde, R., Silva, M. F., Carón, R. W., López Fontana, C. M. (2023). Protective effects of Yerba mate (*IIex paraguariensis*) on prostate cancer development. *Nutrition, 108*. https://doi.org/10.1016/j.nut.2022.111957

Santos, F. N., Cruz, E. P., Fonseca, L. M., Pires, J. B., Diaz, P. S., Dias, A. R. G., & Zavareze, E. R. (2024b). Cassava starch esterification with formic acid for fabrication of electrospun nanofibers. *International Journal of Biological Macromolecules, 266*, Article 131182. https://doi.org/10.1016/j.ijbiomac.2024b.131182

Santos, F. N., de Souza, E. J. D., de Souza, J. F., Pires, J. B., Siebeneichler, T. J., Kringel, D. H., Fajardo, A. R., Rombaldi, C. V., Dias, A. R. G., & da Rosa Zavareze, E. (2023). Encapsulation of anthocyanic extract of jambolan (*Syzygium cumini* (L.)) in zein sub-micron nanofibers produced by electrospinning. *Food Biophysics, 18*(1), 133–147. https://doi.org/10.1007/s11483-022-09758-3

Santos, F. N., Fonseca, L. M., Jansen-Alves, C., Crizel, R. L., Pires, J. B., Kroning, I. S., Souza, J. F., Fajardo, A. R., Lopes, G. V., Dias, A. R. G., & Zavareze, E. R. (2024a). Antimicrobial activity of geranium (*Pelargonium graveolens*) essential oil and its encapsulation in carioca bean starch ultrafine nanofibers by electrospinning. *International Journal of Biological Macromolecules*. https://doi.org/10.1016/j.ijbiomac.2024.130953

Santos, F. N., Souza, E. J. D., Pires, J. B., Crizel, R. L., Cruz, E., Kroning, I. S., Fonseca, L. M., Assis, L. M., Lopes, G. V., Dias, A. R. G., & Zavareze, E. R. (2025). Orange peel essential oil in rice starch encapsulating material for antimicrobial application against *Escherichia coli*. *International Journal of Biological Macromolecules*. https://doi.org/10.1016/j.ijbiomac.2024.138955

Silveira, M. M., Dittgen, C. L., Batista, C. S., Biduski, B., Gutkoski, L. C., & Vanier, N. L. (2020). Discrimination of the quality of Brazilian wheat genotypes and their use as whole-grains in human nutrition. *Food Chemistry, 312*, Article 126074. https://doi.org/10.1016/j.foodchem.2019.126074

Souza, E. J. D., Santos, F. N., Kringel, D. H., Souza, J. F., Bueno, D. T., Leitzke, A. F., Fajardo, A. R., Gandra, E. A., Pereira, C. M. P., Dias, A. R. G., & Zavareze, E. R. (2024). Multivariate optimization for the production of OSA-starch microcapsules containing clove and white thyme essential oils: Antifungal potential against *Penicillium digitatum*. *Polymers for*

Advanced Technologies, 35(12), 1–17. https://doi.org/10.1002/pat.70040

Tarahi, M., Gharagozlou, M., Niakousari, M., & Hedayati, S. (2024). Protein–chlorogenic acid interactions: Mechanisms, characteristics, and potential food applications. *Antioxidants, 13*(7), Article 0777. https://doi.org/10.3390/antiox13070777

Thompson, M., Ellison, S. L., Wood, R. (2002). Harmonized guidelines for single-laboratory validation of methods of analysis (IUPAC Technical Report). Pure and applied chemistry, 74(5), 835-855.

Topuz, F., Uyar, T. (2020). Electrospinning of cyclodextrin nanonanofibers: The effect of process parameters. *Journal of Nanomaterials, 2020*. https://doi.org/10.1155/2020/7529306

Torres, M. R., Pires, J. B., Lemos, G. S., Silva, F. T., Souza, E. J. D., Santos, F. N., Siebeneichler, T. J., Gandra, E. A., Colussi, R., & Zavareze, E. R. (2025). Gelatin film incorporated with pink pepper essential oil: Physical properties and antimicrobial activity through direct contact and micro atmosphere. *Journal of Drug Delivery Science and Technology*. https://doi.org/10.1016/j.jddst.2025.106997

Uecker, J. N., Schneider, J. P., Cerqueira, J. H., Rincón, J. A. A., Campos, F. T., Schneider, A., Barros, C. C., Andreazza, R., Jaskulski, I. B., & Pieniz, S. (2019). *Ilex paraguariensis* extract prevents body weight gain in rats fed a high-fat diet. *Food Science and Technology, 39*(3), 620–626. https://doi.org/10.1590/fst.39817

Unnithan, A. R., Arathyram, R. S., & Kim, C. S. (2015). *Electrospinning of polymers for tissue engineering*. Elsevier Inc. https://doi.org/10.1016/B978-0-323-32889-0.00003-0

Vieira, M. A., Maraschin, M., Amboni, R. D. M. C., Prudêncio, E. S., Pagliosa, C. M., Mantelli, M. B. H., & Amante, E. R. (2023). Thermal condition of mate (*Ilex paraguariensis*) processing. *Ciencia Rural*. https://doi.org/10.1590/0103-8478cr20220178

Wang, C., Chien, H. S., Yan, K. W., Hung, C. L., Hung, K. L., Tsai, S. J., & Jhang, H. J. (2009). Correlation between processing parameters and microstructure of electrospun poly(D,l-lactic acid) nanonanofibers. *Polymer, 50*(25), 6100–6110. https://doi.org/10.1016/j.polymer.2009.10.025

Wang, C., Wang, Y., & Hashimoto, T. (2016). Impact of entanglement density on solution electrospinning: A phenomenological model for fiber diameter. *Macromolecules, 49*(20), 7985–7996. https://doi.org/10.1021/acs.macromol.6b00519

Wang, H., Yang, Q., Ferdinand, U., Gong, X., Qu, Y., Gao, W., Ivanistau, A., Feng, B., & Liu, M. (2020). Isolation and characterization of starch from light yellow, orange, and purple sweet potatoes. *International Journal of Biological Macromolecules, 160*, 660–668. https://doi.org/10.1016/j.ijbiomac.2020.05.259

Yun, P., Devahastin, S., & Chiewchan, N. (2021). Microstructures of encapsulates and their relations with encapsulation efficiency and controlled release of bioactive constituents: A review. *Comprehensive Reviews in Food Science and Food Safety, 20*(2), 1768–1799. https://doi.org/10.1111/1541-4337.12701

Zhang, B., Guo, K., Lin, L., & Wei, C. (2018). Comparison of structural and functional properties of starches from the rhizome and bulbil of Chinese yam (*Dioscorea opposita* Thunb.). *Molecules (Basel, Switzerland), 23*(2), 8–11. https://doi.org/10.3390/molecules23020427

Publisher's Note Springer Nature remains neutral with regard to jurisdictional claims in published maps and institutional affiliations.